Effects of Confinement on Microstructure and Charge Transport in High Performance Semicrystalline Polymer Semiconductors

Scott Himmelberger, Javier Dacuña, Jonathan Rivnay, Leslie H. Jimison, Thomas McCarthy-Ward, Martin Heeney, Iain McCulloch, Michael F. Toney, and Alberto Salleo*

The film thickness of one of the most crystalline and highest performing polymer semiconductors, poly(2,5-bis(3-tetradecylthiophen-2-yl)thieno[3,2-b] thiophene) (PBTTT), is varied in order to determine the effects of interfaces and confinement on the microstructure and performance in organic field effect transistors (OFETs). Crystalline texture and overall film crystallinity are found to depend strongly on film thickness and thermal processing. The angular distribution of crystallites narrows upon both a decrease in film thickness and thermal annealing. These changes in the film microstructure are paired with thin-film transistor characterization and shown to be directly correlated with variations in charge carrier mobility. Charge transport is shown to be governed by film crystallinity in films below 20 nm and by crystalline orientation for thicker films. An optimal thickness is found for PBTTT at which the mobility is maximized in unannealed films and where mobility reaches a plateau at its highest value for annealed films.

1. Introduction

Semiconducting polymers have garnered significant interest in recent years for applications in large-area, low-cost, and flexible electronics.[1] These materials can be processed from solution and are compatible with inexpensive and high-throughput printing and coating deposition techniques.[2,3] Many of the best performing polymer semiconductors exhibit a high degree of order and are typically semicrystalline. In recent years, the field effect mobilities of polymers have begun to rival that of amorphous silicon through the rational design and synthesis of molecules with high degrees of crystallinity and improved molecular packing.[4–8]

In optimizing the electronic properties of semiconducting polymers, much attention has been paid to the semiconductor/substrate interface, where chemical functionalization plays a significant role in controlling the microstructure.[9–13] In many of the applications for semiconducting polymers, such as polymer light emitting diodes,[14] large-area photovoltaics,[15] and transistor arrays for display backplanes,[16] the thickness of the semiconducting polymer is on the order of tens to hundreds of nanometers. During materials deposition, the interface between the semiconducting polymer film and the solvent is unconstrained. Therefore, there is a second interface to consider, namely the semiconductor/solvent interface. Indeed, in very thin films, the semiconductor/solvent interface may affect materials structure all the way to the substrate/semiconductor interface. Furthermore, when a dry film is annealed, the polymer film/air interface is free and its effect on microstructure should be considered as well. The combined effect of these two interfaces on film microstructure is classically examined using film thickness studies. As the polymer film thickness begins to approach very small dimensions, the effects of both interfaces become increasingly important and the microstructure and properties of the film may begin to differ significantly from those of thicker films and may become strongly thickness-dependent.[17] With the thinnest films one might surmise that there is no bulk anymore and the film properties are dominated by the properties of the interfaces. Thus, as organic semiconductors gain more industrial significance, it becomes imperative to have a good understanding of how these materials behave in very thin films.

We investigate the effects of interfaces on the microstructure and charge transport in ultrathin films of the high-performance p-type polymer poly(2,5-bis(3-tetradecylthiophen-2-yl)thieno[3,2-b]thiophene) (PBTTT).[8] PBTTT is one of the highest mobility and most crystalline semiconducting polymers. It also exhibits a liquid crystalline phase transition at elevated temperatures, above which crystallite reorientation and changes in electrical properties are known to occur.[18,19] PBTTT is therefore a model

S. Himmelberger, J. Dacuña, Dr. J. Rivnay, Dr. L. H. Jimison, Prof. A. Salleo
Materials Science and Engineering
476 Lomita Mall, McCullough Building,
Stanford, CA 94305, USA
E-mail: shimmel@stanford.edu
T. McCarthy-Ward, Prof. M. Heeney, Prof. I. McCulloch
Department of Chemistry
Imperial College
London, SW7 2AZ, UK
Dr. M. F. Toney
Stanford Synchrotron Radiation Lightsource
SLAC National Accelerator Laboratory,
Menlo Park, CA 94025, USA

DOI: 10.1002/adfm.201202408

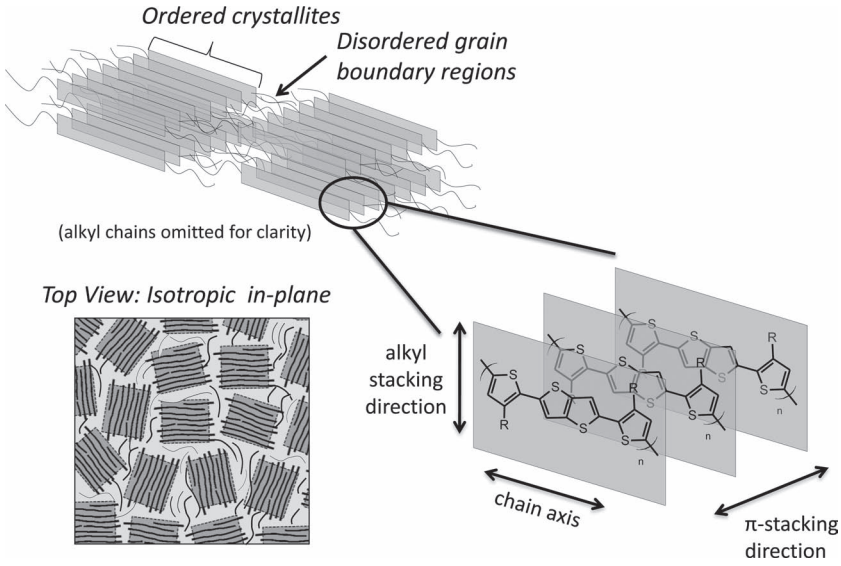

Figure 1. Schematic of lamellar microstructural arrangement of PBTTT (top) including the disordered regions between ordered crystallites. Close-up of molecular packing within ordered crystallites (bottom right) indicating the repeat directions. Top view of spun cast thin films (bottom left) depicting the isotropic distribution of crystallite orientations within the plane of the substrate.

system for this type of study as applied to the more ordered polymers. Previous studies on interface effects have focused on the influence of various surface chemistries on the charge carrier mobility and morphology of polymer thin films. The lateral domain size observed by AFM increased dramatically in films of PBTTT spun on octadecyltrichlorosilane (OTS) compared to bare silicon oxide.[11,12] This change was accompanied by a large improvement in the charge carrier mobility, which was attributed to a reduced density of grain boundaries. A decreased roughness of the gate dielectric was also found to cause a considerable increase in grain size, complemented by an improvement in charge carrier mobility.[20,21]

In addition to the influence of the substrate, the effects of a confined thin film geometry on the crystallization behavior of polymers have also been studied. Disorder was shown to increase significantly in very thin films of poly(3-hexyl)thiophene (P3HT) and charge transport suffered as a result.[22,23] Confinement was also found to reduce crystallinity in very thin films of semicrystalline non-conjugated polymers.[24,25] However, relatively little is known about how these confined geometries affect film morphology in other materials and the resulting changes in the electrical performance of films of conjugated polymers. This work sheds light on these effects by providing the first quantitative measure of crystallinity and crystalline texture in PBTTT. Importantly, quantitative measurements are necessary in order to correlate microstructure to the charge transport properties of PBTTT thin films.

2. Results and Discussion

Isotropic (in the substrate plane) thin films of PBTTT were prepared for X-ray, AFM, and field-effect transistor (FET) device fabrication as described in the experimental section. Film thickness ranged between 5 nm and 100 nm as measured by AFM and confirmed by X-ray reflectivity thickness interference fringes. PBTTT tends to crystallize with the alkyl side chains preferentially oriented out of the plane of the substrate and interdigitated with alkyl chains of adjacent lamellae while the conjugated backbones stack cofacially such that there is significant overlap of pi electron density between polymer chains in what is deemed the pi-stacking direction (**Figure 1**).[26] This orientation is desirable for field effect transistors as fast charge transport occurs along the chain backbone and in the pi-stacking direction which both lie in the plane of the substrate. Using X-ray diffraction measurements, such as pole figure construction,[27] we study the effect of film thickness and thermal annealing on the crystallite orientation and on the degree of crystallinity of PBTTT films. We measure charge carrier mobility in these films using top contact, bottom gate FETs. By studying the effect of interfaces on the crystallization of PBTTT and correlating these findings to FET mobility measurements, we gain insight into the charge transport mechanism in this material. We find that intragranular charge transport between crystalline regions modulates carrier mobility in PBTTT.

Two dimensional grazing incidence X-ray diffraction (GIXD) survey patterns of the spun cast PBTTT films (**Figure 2**a) show the characteristic strong (h00) peaks near the specular, ($q_{xy} = 0$), confirming the preferential lamellar stacking out of the plane of the substrate. Upon annealing at 180 °C (into the liquid crystalline phase), the breadth of the (h00) peaks decreases sharply, coupled with an increase in intensity indicating that the film has become more ordered. AFM micrographs (Figure 2b) also show a dramatic change in the film morphology as the top surface takes on a terraced appearance with lateral domains in the range of 50–200 nm, in agreement with previous findings.[8]

To study the electrical properties of the films, FETs were prepared as described in the experimental section, and mobility measurements were taken for several devices at each thickness (**Figure 3**). In unannealed films, the mobility is highest at a thickness of roughly 30 nm. Away from the maximum, the mobility gradually declines as the film is made thicker and drops off rapidly when the film is made thinner. The annealed films have a higher mobility at nearly all thicknesses and show a similar rapid drop in mobility when the film thickness is below 20 nm. However, unlike the unannealed films, device performance does not suffer when the film is made thicker.

GIXD scans were combined with local specular and high-resolution rocking scans to construct complete pole figures following the methods described previously by Baker et al. and others.[27–30] The (200) peak was chosen for its high intensity as well as ease of subtraction of the diffuse scattering background. The pole figures show a dramatic thickness dependence in the unannealed samples as a significant narrowing of the pole figure is observed as the film is made thinner, indicating that

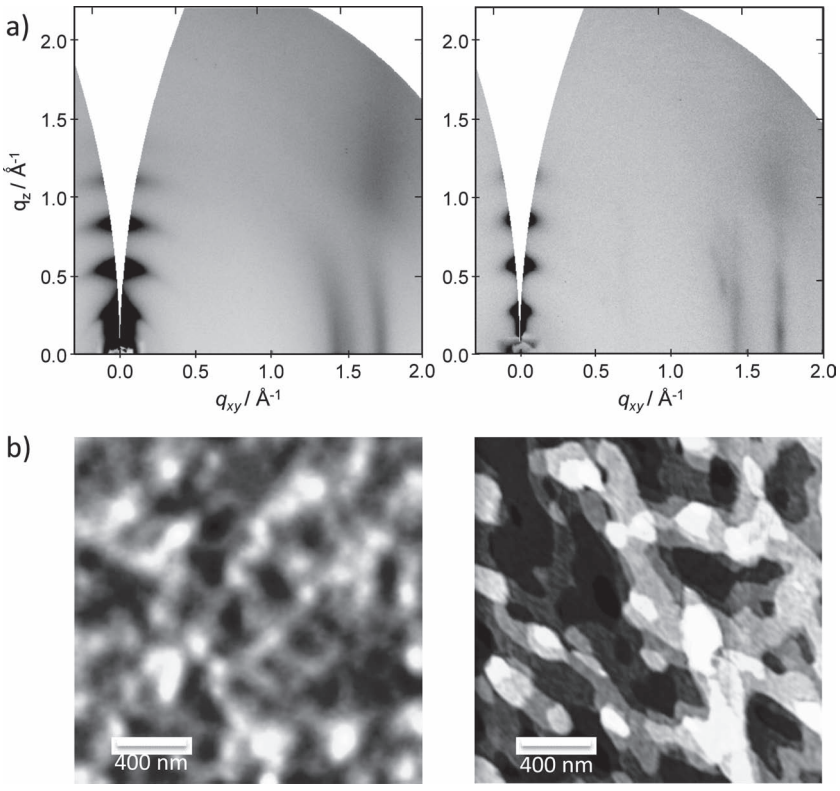

Figure 2. Characterization of PBTTT microstructure, both unannealed (left) and annealed (right) spun cast, isotropic thin films. a) 2D grazing incidence diffraction of ≈20-nm films. b) AFM height mode images of ≈20-nm films.

the fiber texture of the film is improving. Upon annealing, all samples take on a tighter angular distribution of crystallites and the shape of the pole figures does not change significantly with thickness (**Figure 4**a,b). Note the presence of a resolution limited peak (located at $\chi = 0°$). This peak results from perfectly oriented crystallites whose alkyl stacking direction is exactly parallel to the substrate normal,[11] and it increases dramatically upon annealing. By integrating the area under the pole figure (as described in the Supporting Information), the thickness-normalized relative degree of crystallinity (DoC) was calculated for each film (Figure 4c). For the sake of comparison, the DoC of all films is divided by that of the most crystalline film to provide a relative DoC. When the relative DoC is plotted as a function of film thickness, a dramatic drop in crystallinity is observed when film thickness falls below 20 nm for both annealed and unannealed films. Above this thickness the crystallinity is relatively constant with thickness for both the annealed and unannealed films. Despotopoulou et al. observed similar behavior in films of poly(di-*n*-hexylsilane) and suggested that this thickness represents a critical nucleus size for formation of crystallites.[24] Joshi et al. also found a decrease in the degree of crystallinity with decreasing film thickness for the conjugated polymer poly(3-hexylthiophene) (P3HT).[31] The P3HT crystallites were also observed to be much less textured for film thicknesses above 20 nm but become "pinned" such that the alkyl stacking direction is parallel to the substrate normal in thinner films, a similar trend to that observed in PBTTT.[23] Although X-ray diffraction techniques were used to show these trends in P3HT, the changes occurring in texture and DoC were not quantified.

In order to give a description of the angular distribution of crystallites in the film we calculate the integral breadth of the pole figures (Figure 4d). The integral breadth is defined as the width of a rectangle having the same area and the same height as the pole figure (including the resolution limited peak), and provides a measure of the crystallite angular distribution. The integral breadth steadily increases with thickness for the unannealed films, indicating a less preferential angular distribution, as the crystallites have more rotational freedom when they are not pinned between the top and bottom interfaces. We also determined the fraction of the total crystallinity which is perfectly oriented and hence in contact with the dielectric interface, as this is the only surface which could cause the crystallite alkyl stacking direction to be exactly parallel to the substrate normal. In the unannealed films, this perfectly-oriented crystalline fraction is extremely small. This finding agrees with the work of Zhou et al., suggesting that the crystallites do not form when the polymer dries on the substrate but rather that crystalline nuclei are already present in solution and simply precipitate on the substrate during casting.[32] Upon annealing, the integral breadth becomes very narrow at all thicknesses and does not vary significantly with thickness. This change is due in large part to a dramatic increase in the volume fraction of perfectly oriented crystallites, which accounts for close to half of the total film crystallinity in the annealed samples. During the annealing process the distribution of crystallites is no longer kinetically limited and the

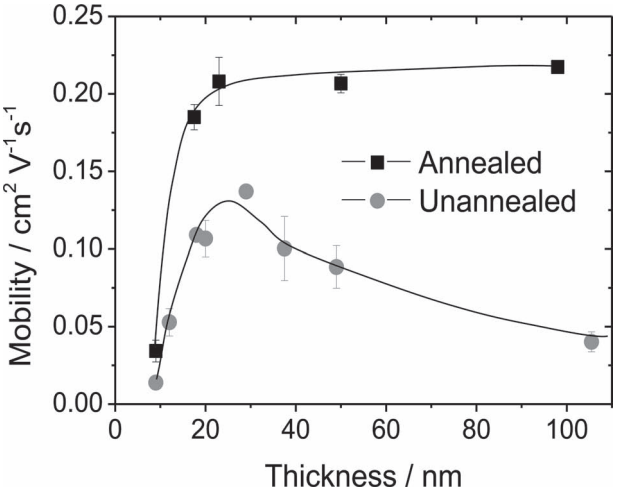

Figure 3. Mobility measurements taken in a bottom-gate FET device architecture for unannealed (grey circles) and annealed (black squares) films as a function of thickness. Thin solid lines are added as a guide for the eye.

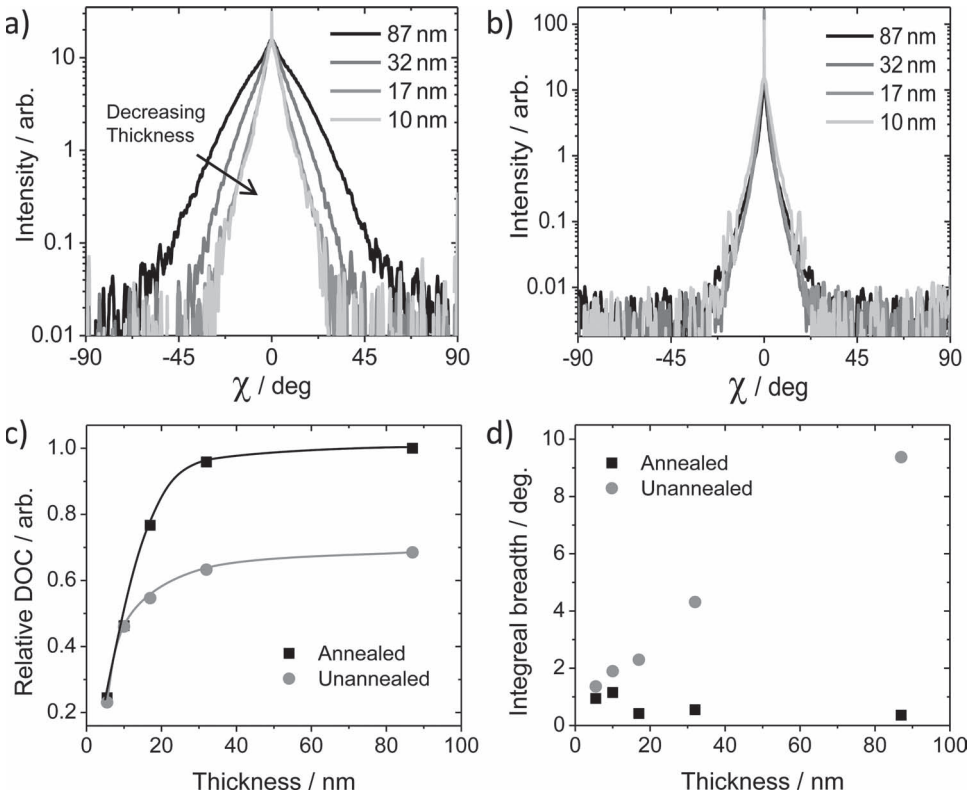

Figure 4. a,b) Pole figures of (200) peak for a series of unannealed (a) and annealed (b) film thicknesses. Peak intensities are normalized with respect to each other for comparison of film textures and are not indicative of total degree of crystallinity. c) Total relative degree of crystallinity normalized to most crystalline film. Thin solid lines are added as a guide for the eye. d) Integral breadth of (200) pole figure.

majority of crystallites reorient with the alkyl stacking direction nearly parallel to the substrate normal. This edge-on packing structure is thought to be thermodynamically favorable for polythiophenes deposited on a silicon dioxide dielectric, although this phenomenon is not well understood.[33,34]

The quantitative analysis of the pole figures also provides insight into the microstructural processes occurring during annealing and how they affect charge transport. Below we will show how crystallites grow through the thickness of the film and reorient to conformations more favorable for charge transport during the annealing process. Using a method related to the analysis of Williamson and Hall we can calculate the crystallite size in the lamellar direction, normal to the substrate surface (Supporting Information Figure S1).[35] For unannealed films the crystallite size matches the film thickness until the film reaches 20 nm. At this point the crystallite size stays constant for thicker films, suggesting a characteristic crystallite size of ≈20 nm for PBTTT in the lamellar direction. This constant crystallite size supports the argument that the crystallites are nucleated in solution and not during the spin-casting process.[32] However, we cannot rule out the possibility that crystallites also form as the solvent evaporates and the solution becomes supersaturated during spin casting. When annealed, the PBTTT crystallite size in the lamellar direction matches the film thickness. Hence upon annealing the crystallites grow from the substrate throughout the film thickness. In films thicker than ≈20 nm, after accounting for the crystallite size in the lamellar direction, the ratio of the perfectly-oriented crystallinity in annealed films to unannealed films is between 20 and 100 (Supporting Information Figure S2). Hence we conclude that upon annealing not only do the crystallites grow throughout the film thicknesses, but more perfectly-oriented crystallites form as well. Since these must be in contact with the substrate, a larger fraction of the substrate/semiconductor interface is covered by perfectly-oriented crystallites. The ratio of the annealed to unannealed perfectly-oriented DoC is:

$$\frac{(DOC)_A}{(DOC)_U} = \frac{(A \times t)_A}{(A \times t)_U}$$

where A is the total area of perfectly-oriented crystallites in the substrate plane and t is the crystallite thickness in the normal direction. The thickness of crystallites in unannealed films is ≈20 nm while that of crystallites in annealed films is equal to the film thickness. For a ≈35 nm film for instance, the intensity arising from the perfectly-oriented peak in annealed films is approximately 65 times that of the unannealed films. However, this number must be normalized by the crystallite thickness, 20 nm for the unannealed film and 35 nm for the annealed film. We conclude that in a 35-nm annealed film the total area of perfectly-oriented crystallites at the substrate/semiconductor interface is ≈40 times larger than in an unannealed film, while the total DoC increases by less than a factor of two. This fact is a likely indication that during annealing crystallites already present realign to become better oriented with the substrate

leading to a dramatic increase in highly oriented crystallites but not a very large overall crystallinity increase. This reorientation is made possible by the chains in existing crystallites becoming mobile after our annealing to above the liquid crystalline transition temperature of ≈150 °C.[34] As a result, at the interface the local DoC may not increase substantially upon annealing but the relative orientation distribution tightens very significantly.

Our quantitative microstructural analysis allows us to conclude that for unannealed PBTTT films thicker than 20 nm, increasing the film thickness results in broadening the crystallite texture. Annealing such films on the other hand mainly results in reorienting those crystallites and dramatically decreases their texture breadth. Only a modest increase in the overall DoC however is observed upon annealing.

In ultrathin films (thickness <20 nm) on the other hand, the pole figure measurements indicate that the DoC of PBTTT is strongly suppressed. This effect is much more pronounced in annealed films, where the relative DoC drops by a factor of ≈4 when the film thickness changes from 32 nm to 5.5 nm. In unannealed films, a 32 nm film is ≈2.5 times more crystalline than a 5.5 nm film. The thickness at which crystallinity begins to drop in PBTTT closely matches the characteristic crystallite size (≈20 nm) found in unannealed films. Frank et al. observed a similar phenomenon in ultrathin films of a non-conjugated semicrystalline polymer with a comparable characteristic crystallite size. This suppression in crystallinity was attributed to a critical nucleus thickness needed for ordered crystallite formation.[25,36] The drop in PBTTT crystallinity for films below 20 nm is likely due to a similar phenomenon. In PBTTT films below approximately 10-nm thick, the total DoC does not change significantly with annealing, however the crystallite orientation distribution becomes slightly narrower. This data suggests that during annealing in ultra-thin films, the formation of new crystallites and the growth of preexisting crystallites is strongly suppressed due to the presence of the interfaces, but the crystallites already present have the ability to rearrange their orientation to a more energetically favorable microstructure, as observed in thicker films.

Having characterized the microstructure of PBTTT films as a function of thickness and thermal treatment, we measured the charge transport properties of these films. The thickness dependence of mobility in the unannealed films provides insight into the factors limiting charge transport. Indeed, the mobility in unannealed films drops from ≈0.14 $cm^2/V \cdot s$ for 30 nm films to ≈0.04 $cm^2/V \cdot s$ in 90 nm films. The overall DoC is constant for unannealed films thicker than 30 nm (Figure 4c) suggesting that the local DoC at the semiconductor/dielectric interface is also constant in all these films, as observed with the perfectly-oriented fraction and supported by the fact that these films are all thicker than the characteristic crystallite thickness (≈20 nm). The constant DoC as a function of thickness is in agreement with the hypothesis that crystallites do not form on the substrate during drying. Furthermore, no major morphology difference is observed by AFM as a function of thickness. Moreover, in-plane coherence length estimates were performed for all films as a measure of crystallite quality in one of the fast transport directions. These were obtained from the FWHM of the pi-stacking peak (Supporting Information Figure S3).[37,38] The coherence length in the π-stacking direction is essentially constant at all film thicknesses and therefore cannot be the cause of the mobility decrease. Additionally, no correlation is observed between highly oriented crystallinity and charge carrier mobility suggesting that the highly oriented crystallites (which are a small fraction of the film anyway) are not the limiting factor in charge transport. The integral breadth of unannealed films on the other hand varies strongly as a function of thickness, from 2° in 20-nm-thick films to 9° in 90-nm-thick films. The integral breadth calculated for each thickness is a good description of how the crystallites are oriented with respect to each other throughout the film. A similar orientation distribution is likely found in close proximity to the polymer-dielectric interface as well. The hypothesis that crystallites nucleate in solution indicates that the primary effect of the interfaces on texture is to confine the angular distribution of crystallites during spin coating. It is therefore expected that while changing the film thickness affects the distribution of crystallite orientations, this distribution will be relatively constant throughout the thickness of the film.

Transport models suggest the electronic properties of the boundary between two adjacent grains depend primarily on their relative orientation.[39] This model is supported by the large anisotropy of charge transport due to misaligned grain boundaries found in aligned polythiophene thin films.[40–42] Our observation of a gradual decrease in mobility (as deposited films) as the integral breadth of crystallites increases in progressively thicker films of PBTTT strongly suggests that intergranular transport limits carrier mobility in unannealed films. Films with a broader distribution of crystallite orientations show a lower mobility due to the increased misalignment between neighboring crystallites and the suppression of charge transport that accompanies this. Indeed, as a result of the larger misorientation, the number of percolating paths available to charges is diminished.

Upon annealing films thicker than 20 nm, on the other hand, the density of perfectly-oriented crystallites at the interface increases dramatically. This increase is due to a microstructural rearrangement where crystallites reorient more favorably for charge transport. Such rearrangement is accompanied by a mobility increase upon annealing, which suggests that intergranular transport governs mobility in PBTTT. Because the dielectric/semiconductor interface is the same for all thicknesses after this reorientation process, field-effect mobility does not depend on film thickness in annealed PBTTT films.

In order to confirm these microstructure-mobility correlations, we performed a series of measurements of temperature-dependent current-voltage characteristics of TFTs to better understand what led to the changes in charge transport. The measurements were fit to the mobility edge (ME) model. Details of the model, implementation, and fitting procedure can be found elsewhere.[43–51] Briefly, in the ME model, charges are divided into mobile holes, with a mobility μ_0, and holes trapped in an exponential distribution of states having a characteristic depth E_b and a density N_t. ME model parameters were obtained by least-squares fitting a set of temperature-dependent transfer curves. A typical transfer curve representative of all devices, showing excellent agreement with the ME model, is shown in **Figure 5**. The results of the modeling show an increase of the parameter μ_0 upon annealing. Furthermore, μ_0 decreases

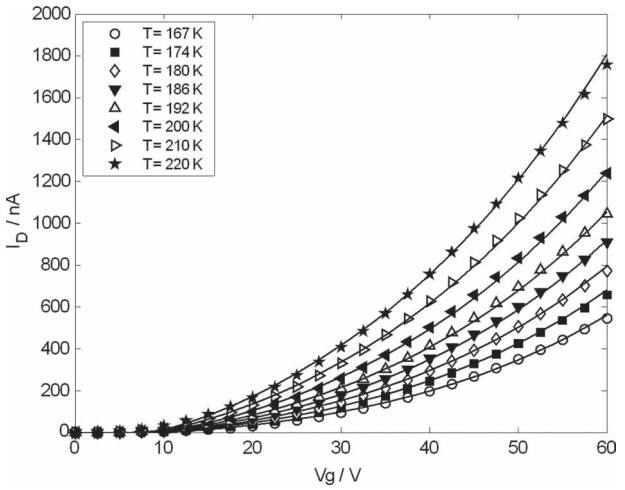

Figure 5. Transfer curves (points) and ME model fit (lines) of 105 nm unannealed PBTTT film for $V_D = -5$ V.

in unannealed films as they are made thicker. On the other hand, the total density of traps, N_t, remains relatively constant (**Table 1**). The modeling results are consistent with an enhancement of the film conductivity due to an increase of the number of percolation paths caused by the reorientation of crystallites near the semiconductor-dielectric interface, while the overall crystalline quality remains unaffected. Indeed, μ_0 reflects the trap-free mobility of charges, which must correlate positively with the number of available transport paths.

In films thinner than 20 nm on the other hand, charge carrier transport is not limited by crystallite orientation. Recall that in films thinner than 20 nm, both annealed and unannealed, the mobility decreases as film thickness is decreased while texture does not change significantly with thickness. From these trends we conclude that charge carrier transport is not limited by crystallite orientation, but by degree of crystallinity. While the absolute degree of crystallinity is not known, it is reasonable to assume that because the thinner films are 20–80% as crystalline as the most crystalline films, we are in a regime close to the percolation limit for crystallites. In this region one would expect the mobility to depend strongly on DoC. Although the scaling of mobility with DoC is expected to be quite complicated, and other factors such as crystalline perfection may intervene, the observed mobility does drop sharply in thinner films.

The thickness dependent morphological and electrical behavior of PBTTT shows some similarity to that of P3HT as well as several distinct differences. Joshi et al. found an improvement in crystalline texture as well as a decrease in crystallinity as the film thickness was lowered in P3HT.[23,52] Additionally, they found a relatively constant mobility with film thickness, except for a large drop in mobility for very thin films (<10 nm) which was attributed to an increase in disorder. While morphologically this behavior is similar to the unannealed PBTTT samples, PBTTT displays a peak in mobility before dropping off again in thicker films. We attribute this difference to the higher inherent crystallinity of PBTTT. As more of the film volume is composed of crystalline material, such as in the case of PBTTT, the connections between crystallites, especially their dependence on relative orientations, become increasingly important. In P3HT on the other hand, non-crystalline aggregates play a more important role and as a result the orientation of the crystallites with respect to each other does not affect mobility as significantly as in unannealed PBTTT as long as the texture is predominantly edge-on. PBTTT also displays unique behavior not found in P3HT due to the fact that it can be annealed into a liquid crystalline phase. Crystallites were found to exhibit a characteristic size (≈20 nm) in unannealed films of PBTTT that grew throughout the film thickness during thermal annealing, while the crystallite size in P3HT was found to generally increase with thickness but did not show any strong correlation or characteristic size.[23] After annealing, PBTTT displays a similar mobility trend to as-cast P3HT, but the constant mobility in thicker films of PBTTT is due to the rearrangement and growth of perfectly-oriented crystallites at the semiconductor-dielectric interface, a process which cannot be mimicked in P3HT. Together, these two materials provide useful insight into many of the different factors affecting charge transport in semicrystalline polymer semiconductors.

Table 1. Mobility Edge model parameters obtained for different film thicknesses and annealing conditions.

	μ_0 [cm^2/Vs]	E_b [meV]	N_t [cm^{-2}]	D_{band} [cm^{-2}]
20 nm unnanealed	3.8	31	2.0×10^{-13}	2×10^{14}
20 nm annealed	6.6	32	1.8×10^{13}	2×10^{14}
105 nm unannealed	0.7	32	1.7×10^{13}	2×10^{14}

3. Conclusions

In conclusion, we have investigated the effects of interfaces on the microstructure and charge carrier mobility in thin films of PBTTT. Film texture is significantly affected by the presence of interfaces in unnannealed films while in annealed films crystallites rearrange and grow through the thickness of the film leading to similar textures for all film thicknesses. By correlating our microstructural characterization with transport measurements we demonstrate that the high carrier mobility in PBTTT is due not only to the material's inherent crystallinity, but more importantly to the well oriented crystallites within the film which allow charges to travel easily between neighboring crystalline domains. When the film thickness drops below a certain critical value, the formation of crystallites is strongly inhibited and the charge carrier mobility drops due to the decrease in crystalline fraction. In unannealed films thicker than 20 nm or ultrathin films–both annealed and unannealed–ultimately transport is always governed by percolation through crystallites. If there is an abundance of crystallites (e.g., unannealed films thicker than 20 nm), the number of percolating paths is controlled by crystalline texture. If there is scarcity of crystallites, the number of percolating paths is controlled by crystallite density. The different thickness-dependence of these two factors (crystallite density and crystallite orientation) leads to an optimal PBTTT thickness at which mobility is maximized

in both unnannealed and annealed films. It should be emphasized that uncovering such correlations is only possible because quantitative X-ray measurements are used throughout this work.

This work suggests that for many of the applications in which polymer semiconductors are used, film thickness is of critical importance. Increasing the active layer thickness not only requires the use of more material, but it may ultimately inhibit device performance. Efforts into improving performance of electronic devices should therefore not focus solely on developing new materials and testing them in bulk, but should also consider how these materials interact with interfaces and form films in confined geometries.

4. Experimental Section

Materials: Poly(2,5-bis(3-tetradecylthiophen-2-yl)thieno[3,2-b]thiophene), (PBTTT-C14), (M_n = 22 kDa, M_w = 44 kDa), was prepared as previously described.[8]

Film Fabrication: Isotropic films were spun cast from solution (1–20 mg mL^{-1}) from 1,2-dichlorobenzene (DCB) at 1200 rpm. Annealed films were heated on a hot plate at 180 °C for 20 min. Films used for XRD were spun on silicon with native oxide; those for devices were prepared as described below. All substrates were treated with an octadecyltrichlorosilane (OTS) self assembled monolayer after a 20 min UV-ozone treatment. Spun film preparation was done in a N_2 glove box (<1 ppm O_2).

X-Ray and AFM Characterization: X-ray scattering was performed at the Stanford Synchrotron Radiation Lightsource (SSRL) on beam line 7-2 (high resolution grazing incidence), 2-1 (high resolution specular data), and 11-3 (2D scattering with an area detector, MAR345 image plate, at grazing incidence). The incident energy was 8 keV for beam lines 7-2 and 2-1, and 12.7 keV for beam line 11-3. The diffracted beam was collimated with 1 milliradian Soller slits for high resolution in-plane scattering and with two 1mm slits for specular diffraction. For both grazing incidence experiments, the incidence angle was slightly larger than the critical angle, ensuring that we sampled the full film depth. Scattering data are expressed as a function of the scattering vector $q = 4\pi\sin(\theta)/\lambda$, where θ is half the scattering angle and λ is the wavelength of the incident radiation. Here, q_{xy} (q_z) is the component of the scattering vector parallel (perpendicular) to the substrate. AFM characterization was performed with a PARC Systems XE-70, in noncontact mode.

Transistor Fabrication and Testing: Films for device characterization were spun on Si substrates with a 200-nm layer of thermally grown oxide treated with an OTS self assembled monolayer. After spinning the active layer, thermally evaporated gold source and drain contacts were deposited. Relatively long channel lengths of 70–200 µm were used to avoid contact resistance effects. Mobility was evaluated in the linear regime for 4-5 devices per thickness.

Supporting Information

Supporting Information is available from the Wiley Online Library or from the author.

Acknowledgements

Portions of this research were carried out at the Stanford Synchrotron Radiation Lightsource, a national user facility operated by Stanford University on behalf of the US Department of Energy, Office of Basic Energy Sciences. A.S. and S.H. gratefully acknowledge financial support from the National Science Foundation. This publication was partially based on work supported by the Center for Advanced Molecular Photovoltaics (Award No. KUS-C1-015-21), made by King Abdullah University of Science and Technology (KAUST).

Received: August 23, 2012
Revised: October 12, 2012
Published online: November 23, 2012

[1] A. C. Arias, J. D. MacKenzie, I. McCulloch, J. Rivnay, A. Salleo, *Chem. Rev.* **2010**, *110*, 3–24.
[2] J. Bharathan, Y. Yang, *Appl. Phys. Lett.* **1998**, *72*, 2660–2662.
[3] T. R. Hebner, C. C. Wu, D. Marcy, M. H. Lu, J. C. Sturm, *Appl. Phys. Lett.* **1998**, *72*, 519–521.
[4] H. Sirringhaus, P. J. Brown, R. H. Friend, M. M. Nielsen, K. Bechgaard, B. M. W. Langeveld-Voss, A. J. H. Spiering, R. a. J. Janssen, E. W. Meijer, P. Herwig, D. M. de Leeuw, *Nature* **1999**, *401*, 685–688.
[5] B. S. Ong, Y. Wu, P. Liu, S. Gardner, *J. Am. Chem. Soc.* **2004**, *126*, 3378–3379.
[6] B. H. Hamadani, D. J. Gundlach, I. McCulloch, M. Heeney, *Appl. Phys. Lett.* **2007**, *91*, 243512.
[7] H. Yan, Z. Chen, Y. Zheng, C. Newman, J. R. Quinn, F. Dötz, M. Kastler, A. Facchetti, *Nature* **2009**, *457*, 679–686.
[8] I. McCulloch, M. Heeney, C. Bailey, K. Genevicius, I. MacDonald, M. Shkunov, D. Sparrowe, S. Tierney, R. Wagner, W. Zhang, M. L. Chabinyc, R. J. Kline, M. D. McGehee, M. F. Toney, *Nat. Mater.* **2006**, *5*, 328–333.
[9] A. Salleo, M. L. Chabinyc, M. S. Yang, R. A. Street, *Appl. Phys. Lett.* **2002**, *81*, 4383–4385.
[10] R. J. Kline, D. M. DeLongchamp, D. A. Fischer, E. K. Lin, M. Heeney, I. McCulloch, M. F. Toney, *Appl. Phys. Lett.* **2007**, *90*, 062117.
[11] R. J. Kline, M. D. McGehee, M. F. Toney, *Nat. Mater.* **2006**, *5*, 222–228.
[12] M. L. Chabinyc, M. F. Toney, R. J. Kline, I. McCulloch, M. Heeney, *J. Am. Chem. Soc.* **2007**, *129*, 3226–3237.
[13] I. McCulloch, M. Heeney, M. L. Chabinyc, D. DeLongchamp, R. J. Kline, M. Cölle, W. Duffy, D. Fischer, D. Gundlach, B. Hamadani, R. Hamilton, L. Richter, A. Salleo, M. Shkunov, D. Sparrowe, S. Tierney, W. Zhang, *Adv. Mater.* **2009**, *21*, 1091–1109.
[14] J. H. Burroughes, D. D. C. Bradley, A. R. Brown, R. N. Marks, K. Mackay, R. H. Friend, P. L. Burns, A. B. Holmes, *Nature* **1990**, *347*, 539–541.
[15] C. W. Tang, *Appl. Phys. Lett.* **1986**, *48*, 183–185.
[16] A. C. Arias, S. E. Ready, R. Lujan, W. S. Wong, K. E. Paul, A. Salleo, M. L. Chabinyc, R. Apte, R. A. Street, Y. Wu, P. Liu, B. Ong, *Appl. Phys. Lett.* **2004**, *85*, 3304–3306.
[17] J. H. van Zanten, W. E. Wallace, W. Wu, *Phys. Rev. E* **1996**, *53*, R2053–R2056.
[18] B. A. Collins, J. E. Cochran, H. Yan, E. Gann, C. Hub, R. Fink, C. Wang, T. Schuettfort, C. R. McNeill, M. L. Chabinyc, H. Ade, *Nat. Mater.* **2012**, *11*, 536–543.
[19] X. Zhang, S. D. Hudson, D. M. DeLongchamp, D. J. Gundlach, M. Heeney, I. McCulloch, *Adv. Funct. Mater.* **2010**, *20*, 4098–4106.
[20] M. L. Chabinyc, R. Lujan, F. Endicott, M. F. Toney, I. McCulloch, M. Heeney, *Appl. Phys. Lett.* **2007**, *90*, 233508.
[21] Y. Jung, R. J. Kline, D. A. Fischer, E. K. Lin, M. Heeney, I. McCulloch, D. M. DeLongchamp, *Adv. Funct. Mater.* **2008**, *18*, 742–750.
[22] B. Gburek, V. Wagner, *Org. Electron.* **2010**, *11*, 814–819.
[23] S. Joshi, S. Grigorian, U. Pietsch, P. Pingel, A. Zen, D. Neher, U. Scherf, *Macromolecules* **2008**, *41*, 6800–6808.
[24] M. M. Despotopoulou, C. W. Frank, R. D. Miller, J. F. Rabolt, *Macromolecules* **1995**, *28*, 6687–6688.

[25] C. W. Frank, V. Rao, M. M. Despotopoulou, R. F. W. Pease, W. D. Hinsberg, R. D. Miller, J. F. Rabolt, *Science* **1996**, *273*, 912–915.
[26] D. M. DeLongchamp, R. J. Kline, E. K. Lin, D. A. Fischer, L. J. Richter, L. A. Lucas, M. Heeney, I. McCulloch, J. E. Northrup, *Adv. Mater.* **2007**, *19*, 833–837.
[27] J. L. Baker, L. H. Jimison, S. Mannsfeld, S. Volkman, S. Yin, V. Subramanian, A. Salleo, A. P. Alivisatos, M. F. Toney, *Langmuir* **2010**, *26*, 9146–9151.
[28] L. H. Jimison, Ph.D. Thesis, Stanford University, **2011**.
[29] B. W. Boudouris, V. Ho, L. H. Jimison, M. F. Toney, A. Salleo, R. A. Segalman, *Macromolecules* **2011**, *44*, 6653–6658.
[30] J. Rivnay, R. Steyrleuthner, L. H. Jimison, A. Casadei, Z. Chen, M. F. Toney, A. Facchetti, D. Neher, A. Salleo, *Macromolecules* **2011**, *44*, 5246–5255.
[31] S. Joshi, S. Grigorian, U. Pietsch, *Phys. Status Solidi A* **2008**, *205*, 488–496.
[32] L.-H. Zhao, R.-Q. Png, J.-M. Zhuo, L.-Y. Wong, J.-C. Tang, Y.-S. Su, L.-L. Chua, *Macromolecules* **2011**, *44*, 9692–9702.
[33] D. M. DeLongchamp, B. M. Vogel, Y. Jung, M. C. Gurau, C. A. Richter, O. A. Kirillov, J. Obrzut, D. A. Fischer, S. Sambasivan, L. J. Richter, E. K. Lin, *Chem. Mater.* **2005**, *17*, 5610–5612.
[34] D. M. DeLongchamp, R. J. Kline, Y. Jung, E. K. Lin, D. A. Fischer, D. J. Gundlach, S. K. Cotts, A. J. Moad, L. J. Richter, M. F. Toney, M. Heeney, I. McCulloch, *Macromolecules* **2008**, *41*, 5709–5715.
[35] G. K. Williamson, W. H. Hall, *Acta Metall.* **1953**, *1*, 22–31.
[36] M. M. Despotopoulou, C. W. Frank, R. D. Miller, J. F. Rabolt, *Macromolecules* **1996**, *29*, 5797–5804.
[37] J. Rivnay, R. Noriega, J. E. Northrup, R. J. Kline, M. F. Toney, A. Salleo, *Phys. Rev. B* **2011**, *83*, 121306.
[38] J. Rivnay, R. Noriega, R. J. Kline, A. Salleo, M. F. Toney, *Phys. Rev. B* **2011**, *84*, 045203.
[39] A. Salleo, T. W. Chen, A. R. Völkel, Y. Wu, P. Liu, B. S. Ong, R. A. Street, *Phys. Rev. B* **2004**, *70*, 115311.
[40] L. H. Jimison, M. F. Toney, I. McCulloch, M. Heeney, A. Salleo, *Adv. Mater.* **2009**, *21*, 1568–1572.
[41] M. J. Lee, D. Gupta, N. Zhao, M. Heeney, I. McCulloch, H. Sirringhaus, *Adv. Funct. Mater.* **2011**, *21*, 932–940.
[42] E. J. W. Crossland, K. Tremel, F. Fischer, K. Rahimi, G. Reiter, U. Steiner, S. Ludwigs, *Adv. Mater.* **2012**, *24*, 839–844.
[43] J.-F. Chang, H. Sirringhaus, M. Giles, M. Heeney, I. McCulloch, *Phys. Rev. B* **2007**, *76*, 205204.
[44] W. L. Kalb, B. Batlogg, *Phys. Rev. B* **2010**, *81*, 035327.
[45] W. L. Kalb, S. Haas, C. Krellner, T. Mathis, B. Batlogg, *Phys. Rev. B* **2010**, *81*, 155315.
[46] D. Oberhoff, K. P. Pernstich, D. J. Gundlach, B. Batlogg, *IEEE Trans. Electron Devices* **2007**, *54*, 17–25.
[47] K. P. Pernstich, B. Rössner, B. Batlogg, *Nat. Mater.* **2008**, *7*, 321–325.
[48] H. Sirringhaus, *Adv. Mater.* **2005**, *17*, 2411–2425.
[49] H. Xie, H. Alves, A. F. Morpurgo, *Phys. Rev. B* **2009**, *80*, 245305.
[50] N. Zhao, Y.-Y. Noh, J.-F. Chang, M. Heeney, I. McCulloch, H. Sirringhaus, *Adv. Mater.* **2009**, *21*, 3759–3763.
[51] D. P. McMahon, D. L. Cheung, L. Goris, J. Dacuña, A. Salleo, A. Troisi, *J. Phys. Chem. C* **2011**, *115*, 19386–19393.
[52] S. Joshi, P. Pingel, S. Grigorian, T. Panzner, U. Pietsch, D. Neher, M. Forster, U. Scherf, *Macromolecules* **2009**, *42*, 4651–4660.